Synthesis of Molecular Adducts of Beryllium, Boron, and Gallium Cyanides: Theoretical and Experimental Correlations between Solid-State and Molecular Analogues

A. V. G. Chizmeshya, C. J. Ritter, T. L. Groy, J. B. Tice, and J. Kouvetakis*

Department of Chemistry and Biochemistry, Arizona State University, Tempe, Arizona 85287-1604

Received May 10, 2007. Revised Manuscript Received August 14, 2007

Metal cyanide framework materials with stoichiometries $M(CN)_2$ and $M'(CN)_3$ represent an intriguing family of inclusion compounds with technological potential in materials science and energy storage applications. In this paper we develop fundamental new insights by comparing, experimentally and theoretically, the structure and bonding trends in several molecular and solid-state main group compounds containing the same basic M—C≡N "building blocks". In particular we describe for the first time the synthesis and structural characterization of molecular analogues of the $Be(CN)_2$ and $Ga(CN)_3$ frameworks such as $Be(CN)_2(NC_5H_5)_2$ and $Ga(CN)_3(NC_5H_5)_2$, which represent prototypical examples of simple binary cyanides of the main group element class. We also describe the formation of closely related analogues of boron such as $B(CN)_3 \cdot NC_5H_5$ and $B(CN)_4 \cdot HNC_5H_5$ and report their molecular crystal structures. Complementary density functional theory simulations are then used to elucidate: (i) the origin of the structural differences between the $Ga(CN)_3(NC_5H_5)_2$ and the corresponding $Ga(CN)_3$ framework solid, (ii) bonding and energetic trends in the $M(CN)_3(NC_5H_5)_2$ series of molecules (M = Al, Ga, In), (iii) deviations from idealized structure in the M—CN—M units within the framework solids, and (iv) bond distributions in orientationally disordered framework solids.

Introduction

There is an ongoing interest in C—N metal framework compounds due to their unique fundamental properties and significant practical potential as porous inclusion materials exhibiting ideal $M(CN)_3$ stoichiometries and octahedral coordination.[1–5] In this connection a considerable body of work has also been focused on the study of symmetrical and asymmetrical tetrahedral analogues with formulas $M^{II}(CN)_2$ and $M^{I}M^{III}(CN)_4$, respectively.[6–10] Our prior activity in this arena has involved the synthesis and detailed characterization of a broad range of main group metal phases in this class of solid-state materials including $M(CN)_3$ (M = B, Al, Ga, and In), $Mg(CN)_2$, $Be(CN)_2$ $(Tl^{I},Tl^{III})(CN)_2$, $LiB(CN)_4$, and $LiGa(CN)_4$ as well as a number of random alloys based on combinations of binary systems.[4–8] Our early studies were motivated by the quest for ultrahard light-element compounds that are isolectronic to diamond or possess the C_3N_4/Si_3N_4 structure.[11,12] Examples include the BeC_2N_2 and BC_3N_3 systems which were specifically targeted as precursors for the subsequent synthesis of advanced light-element ceramics via high pressure or laser ablation processing.[6,8] Further work on these compounds has recently prompted first principles studies, which have shown that $Al(CN)_3$, $Ga(CN)_3$, and $B(CN)_3$ might exhibit interesting polymorphic behavior and unique physical properties.[13,14]

The common structural theme in all of the above solid-state cyanides involves metal atom sites surrounded by bridging C≡N units. In the prototypical cases of $Be(CN)_2$ and $Ga(CN)_3$ the frameworks comprise corner-shared $Be(C,N)_4$ tetrahedra and $Ga(C,N)_6$ octahedra, respectively, in which the connecting C—N groups are orientationally disordered with respect to the Be/Ga centers.[4,8] The resultant bonding configurations exhibit slight but systematic departures from normal values of bond angles and unresolved bond alignment within the extended structure, and these anomalies might have a significant effect on the zeolitic properties and inclusion behavior including their compressibility to form novel polymorphs. This may have profound implications for their potential use as structural storage materials.[1,15]

* Author to whom correspondence should be addressed: e-mail, jkouvetakis@asu.edu.

(1) Kaye, S. S.; Long, J. R. *Catal. Today* **2007**, *120*, 311.
(2) Kaye, S. S.; Long, J. R. *J. Am. Chem. Soc.* **2005**, *127*, 6506.
(3) Pretsch, T.; Chapman, K. W.; Halder, G. J.; Kepert, C. J. *Chem. Commun.* **2006**, *1857*, 1857.
(4) Brousseau, L. C.; Williams, D.; Kouvetakis, J.; O'Keeffe, M. *J. Am. Chem. Soc.* **1997**, *119*, 6292.
(5) Williams, D.; Kouvetakis, J.; O'Keeffe, M. *Inorg. Chem.* **1998**, *37*, 4617.
(6) Williams, D.; Pleune, B.; Kouvetakis, J.; Williams, M. D.; Anderson, R. A. *J. Am. Chem. Soc.* **2000**, *122*, 7735.
(7) Williams, D.; Partin, D. E.; Lincoln, F. J.; Kouvetakis, J.; O'Keeffe, M. *J. Solid State Chem.* **1997**, *134*, 164.
(8) Williams, D.; Pleune, B.; Leinenweber, C.; Kouvetakis, J. *J. Solid State Chem.* **2001**, *159*, 244.
(9) Batten, S. R.; Robson, R. *Angew. Chem., Int. Ed.* **1998**, *37* (11), 1461.
(10) (a) Küppersa, T.; Köckerlingb, M.; Willner, H. *Z. Anorg. Allg. Chem.* **2007**, *633*, 280. (b) Bernhardt, E.; Henkel, G.; Willner, H. *Z. Anorg. Allg. Chem.* **2000**, *626*, 560. (c) Berkei, M.; Bernhardt, E.; Schürmann, M.; Mehring, M.; Willner, H. *Z. Anorg. Allg. Chem.* **2002**, *628*, 1734.
(11) Liu, A.; Cohen, M. L. *Phys. Rev. Lett.* **1990**, *245*, 841.
(12) Teter, D. M.; Hemley, R. J. *Science* **1996**, *271*, 53.
(13) Betranhandy, E.; Matar, S. F.; Weihrich, R.; Demazeau, G. *C. R. Chim.* **2004**, *7*, 529.
(14) Matar, S. F.; Betranhandy, E.; Nakhl, M. *J. Alloys Compd.* **2007**, *427*, 61.
(15) Goodwin, A. L.; Kepert, C. J. *Phys. Rev.* **2005**, *71*, 140301.

10.1021/cm071275h CCC: $37.00
Published on Web 10/19/2007

To explore the origin of these issues the present work combines experimental and theoretical studies to prepare and describe model molecular analogues of the previously synthesized solids. These molecules harbor the same basic M—C≡N cores as the solids, and a thorough understanding of their fundamental structure and stability is needed to design new families of framework solids based on these materials. Accordingly we have focused on producing representative monomeric $Be(CN)_2(NC_5H_5)_2$ and $Ga(CN)_3(NC_5H_5)_2$ molecular crystals containing pyridine coordinating groups and the classic $Be(CN)_2$ and $Ga(CN)_3$ molecular cores. These incorporate terminal C—N ligands and a highly coordinated central core to closely mimic the local geometry in the corresponding framework solids. First principle simulations were used to corroborate the single-crystal structural analysis for $Ga(CN)_3(NC_5H_5)_2$. This approach was then expanded to the entire sequence of the $M(CN)_3(NC_5H_5)_2$ (M = Al, Ga, In) molecular species as well as the corresponding $M(CN)_3$ solids, to obtain a fresh insight into the fundamental bonding and electronic properties of these materials.

Historically we first explored the creation of Lewis acid–base molecular cyanide adducts with the formation of the $B(CN)_3NCSiMe_3$. The latter was found to thermally decompose, via elimination of Me_3SiCN, to yield polycrystalline BC_3N_3 which is not structurally related to cubic $Al(CN)_3$.[6] The $B(CN)_3NCSiMe_3$ intermediate was prepared via reactions of $B(SCH_3)_3$ and Me_3SiCN. In the present study we have expanded this investigation to develop a more convenient alternative pathway to $B(CN)_3NCSiMe_3$ that affords higher product yields of the material and circumvents the generation of toxic thiomethoxide derivatives. Our experiments to date indicate that the decomposition pathway of $B(CN)_3NCSiMe_3$ to form BC_3N_3 is highly sensitive to minor fluctuations in the reaction conditions leading in some cases to incorporation of impurities, which inhibit formation of crystalline material, and deviations from the ideal BC_3N_3 stoichiometry. We therefore adopted an alternative approach involving displacement of $NCSiMe_3$ from $B(CN)_3NCSiMe_3$ by the more stable NMe_3 Lewis base. This yielded an extremely robust $B(CN)_3NMe_3$ product which does not readily liberate NMe_3 even at high temperatures ultimately leading to the formation of disordered hydrogenated solids (due to the degradation of NMe_3) rather than the desired crystalline form of BC_3N_3. This result suggests that formation of similar coordination compounds with stability intermediate to $B(CN)_3NCSiMe_3$ and $B(CN)_3NMe_3$ might afford tuning of the reactivity and produce suitable precursors.

In this work we have overcome this difficulty by adopting the pyridine coordinating solvent approach (see above), which exploits the weaker basicity and higher thermal stability of the NC_5H_5 ring compared to NMe_3. A reasonable expectation is that pyridine complexes could lead to sublimable solids that decompose via complete loss of the ligand thus avoiding C—H contamination in disproportionation experiments. To explore this concept we first synthesized molecular $B(CN)_3NC_5H_5$. En route to this compound, an unexpected and highly stable byproduct $[B(CN)_4]HNC_5H_5$ was also obtained. Both of these were characterized by single-crystal X-ray diffraction (XRD) and revealed the expected coordination chemistry. It is interesting to note that the $[B(CN)_4]HNC_5H_5$ incorporates the well established $[BCN_4]^-$ anion which was unequivocally identified in the recent synthesis of $LiB(CN)_4$ and by numerous subsequent studies of related compounds.[6,10,16]

This paper is organized as follows. We begin by describing synthetic pathways leading to these pyridine coordinated boron cyanides $B(CN)_3NC_5H_5$ and $[B(CN)_4]HNC_5H_5$. We then discuss the extension of this approach to the synthesis of $Be(CN)_2(NC_5H_5)_2$ and $Ga(CN)_3(NC_5H_5)_2$. The fundamental properties of the latter compound and the hypothetical $Al(CN)_3(NC_5H_5)_2$ and $In(CN)_3(NC_5H_5)_2$ counterparts are investigated and compared by first principle simulations. Experimental and theoretical data are then combined to develop new correlations between these $M(CN)_3(NC_5H_5)_2$ (M = Al, Ga, In) molecular systems and solid-state analogues $M(CN)_3$ on the basis of bond distributions and energies throughout the sequence of compounds considered. This is the first time that main-group cyanides are compared along the molecular/solid-state boundary, and the resultant unified treatment has revealed interesting new insights about cyanide configuration in molecular and extended solid environments.

Results and Discussion

The new synthesis method of $B(CN)_3NCSiMe_3$ involves the reaction of BF_3 with an excess of Me_3SiCN which proceeds via a metathetical exchange resulting in the complete displacement of the fluorines and the formation of $B(CN)_3NCSiMe_3$ in nearly quantitative yields (eq 1).

$$BF_3 + 4Me_3SiCN \rightarrow B(CN)_3NCSiMe_3 + 3Me_3SiF \qquad (1)$$

The identity of $B(CN)_3 \cdot NCSiMe_3$ was confirmed by powder XRD and infrared (IR) spectroscopy, with two sharp absorption bands at 2310 and 2232 cm^{-1} corresponding to bridging cyanide from the coordinating ligand Me_3SiCN and the terminal cyanides of the $B(CN)_3$ fragment, respectively. The synthesis of $B(CN)_3NC_5H_5$ (**1**) is achieved via reactions of $B(CN)_3 \cdot NCSiMe_3$ with an excess of pyridine at 70–75 °C (eq 2).

$$B(CN)_3NCSiMe_3 + NC_5H_5 \rightarrow B(CN)_3NC_5H_5 + Me_3SiCN \qquad (2)$$

The crude product is obtained as a dark oily solid which is dissolved in hot toluene and then cooled to crystallize transparent platelets of the pure compound which are stable in air and melt at 170 °C. The IR spectrum revealed a sharp absorption band centered at 2227 cm^{-1} (C≡N stretch) and characteristic absorption bands due to pyridine coordination. Combustion analysis for C, H, and N is consistent with the proposed $B(CN)_3NC_5H_5$ composition. A single-crystal XRD structure of **1** (Table 1) confirms the formation of a Lewis acid–base complex between NC_5H_5 and $B(CN)_3$. The compound crystallizes in space group $P2_1/n$ with four molecules in the unit cell. Each molecule lies on a crystallographic

(16) Finze, M.; Bernhardt, E.; Willner, H.; Lehmann, C. W. *J. Am. Chem. Soc.* **2005**, *127*, 10712.

Table 1. Crystallographic Data for 1, 2, 3, and 4

formula	$C_8H_5BN_4$ (**1**)	$C_9H_6BN_5$ (**2**)	$C_{12}H_{10}BeN_4$ (**3**)	$C_{13}H_{10}GaN_5$ (**4**)
fw	167.97	195	219.25	305.98
cell Setting	monoclinic	orthorhombic	orthorhombic	triclinic
Space Group	$P2_1/n$	$Pbca$	$Pca2_1$	$P\bar{1}$
crystal color, habit	colorless plate	pale yellow plate	colorless block	colorless block
D(calcd), g cm^{-3}	1.221	1.200	1.224	1.397
a, Å	6.4509(7)	13.2610(9)	17.3618(12)	7.558(4)
b, Å	15.3058(15)	7.6398(5)	8.5384(6)	8.286(4)
c, Å	9.4335(9)	21.3062(14)	8.0293(6)	12.763(6)
α	90.00	90.00	90.00°	77.809(10)
β	101.176(2)	90.00	90.00°	75.389(10)
γ	90.00	90.00	90.00°	71.894(10)
V, Å^3	913.76(16)	2158.6(2)	1189.58(15)	727.5(6)
Z	4	8	4	2
temperature, K	298(2)	298(2)	173(2)	298(2)
R_{obs}	0.0497	0.0470	0.0326	0.0382

Table 2. Crystallographic Bond Length and Bond Angle Data for 1, 2, 3, and 4. The Data Are Arranged To Facilitate a Close Inspection of the Bonding Trends in all Compounds

	$B(CN)_3(NC_5H_5)$	$[B(CN)_4]HNC_5H_5$	$Be(CN)_2(NC_5H_5)_2$	$Ga(CN)_3(NC_5H_5)_2$
		Bond Lengths		
M—C1	1.590	1.580	1.749	2.017
M—C2	1.578	1.597	1.744	2.000
M—C3	1.582	1.594		2.063
M—C4		1.580		
M—N5	1.571		1.764	2.170
M—N6			1.745	2.218
C1—N1	1.133	1.137	1.126	1.076
C2—N2	1.133	1.133	1.115	1.077
C3—N3	1.131	1.135		1.043
C4—N4		1.137		
N5—C5	1.335	1.322	1.333	1.334
C5—C6	1.363	1.341	1.378	1.378
C6—C7	1.362	1.347	1.374	1.363
		Bond Angles		
C1—M—C2	109.41	109.40	114.2	121.2
C2—M—C3	108.34	109.18		122.6
C3—M—C1	107.68	110.32		116.2
C3—M—C4		110.06		
C4—M—C1		108.33		
N5—M—N6			104.7	178.0
M—C1—N1	177.27	178.1	176.6	179.6
M—C2—N2	177.33	179.7	177.2	176.9
M—C3—N3	177.32	179.2		178.6
M—C4—N4		178.5		
M—N5—C5	119.54		123.0	124.6
N5—C5—C6	121.63	119.6	122.9	122.2
C5—C6—C7	119.43	119.1	118.9	119.7

mirror plane with the pyridine ring forming hydrogen bonds with the neighboring cyanide groups.

An ORTEP diagram showing the molecular conformation and the atom numbering scheme is presented in Figure 1.

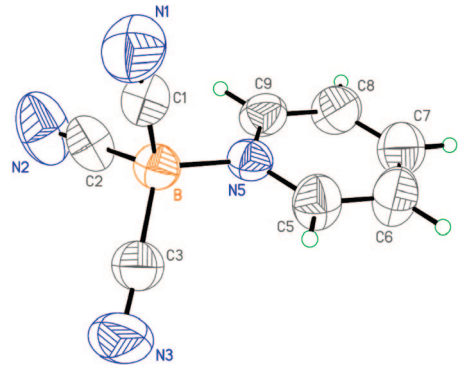

Figure 1. Molecular structure representation of $B(CN)_3NC_5H_5$. The heavy atoms are 50% probability ellipsoids, and the hydrogen atoms are of arbitrary size.

The dative B—N bond distance [1.571(2) Å] and the average B—C bond distances [1.582(6) Å] are nearly identical. The latter are of reasonable value in comparison to other B—C≡N compounds[6–10] while the C—N bond length [1.133(2) Å] is within the range found for similar cyanides[17] but slightly shorter than the C—N length in $LiB(CN)_4$ [1.204(5) Å]. The tetrahedral geometry at the B atom is slightly distorted [108.31(17)–110.33(16)°], and the B—C≡N branches are nearly linear [179.8(3)°]. Selected bond lengths and angles are listed in Table 2.

In addition to the formation of **1**, the above synthesis routinely produces small amounts of a crystalline impurity that was easily separated from **1** on the basis of its distinct crystalline morphology. Single-crystal XRD was used to identify this species as an ionic pyridinium salt in which the $N(H)C_5H_5$ cation is complexed with the $[B(CN)_4]^-$ anion to

(17) Dunbar, K. R.; Heinz, R. A. *Prog. Inorg. Chem.* **1997**, *45*, 283.

form $[B(CN)_4]HNC_5H_5$ (**2**). An ORTEP diagram showing the molecular conformation and the atom numbering scheme is presented in Figure 2. We speculate that the formation of **2** is associated with residual moisture in the solvent which hydrolyzes the coordinating Me_3SiCN ligand of $B(CN)_3NCSiMe_3$ producing Me_3SiOH and an intermediate $[H^+B(CN)_4^-]$ salt. This, in turn, reacts with pyridine leading to **2** as summarized in eq 3.

$$B(CN)_3NCSiMe_3 + H_2O + NC_5H_5 \rightarrow Me_3SiOH + [B(CN)_4]HNC_5H_5 \quad (3)$$

The solid material **2** is recovered as pale yellow platelets which are air stable and crystallize in space group *Pbca* with eight molecules in the unit cell. The B—C bond distances of the $[B(CN)_4]^-$ unit [1.576(3)–1.592(3) Å] are similar to the B—C lengths found for compound **1** and are comparatively close to other 4-fold coordinated boron cyanide compounds.[10] The $[B(CN)_4]^-$ anion exhibits near perfect tetrahedral structure as shown by the relevant bond angles in Table 2. The hydrogen atoms of the pyridinium cation were placed using geometrical considerations and allowed to refine as riding atoms on their bonding partners. The C—N bond length [1.136(2) Å] is virtually identical to that in $B(CN)_3NC_5H_5$ (**1**).

The IR spectrum revealed a sharp absorption band centered at 3244 cm^{-1} and a weak absorption band at 2228 cm^{-1}, attributed to the characteristic N—H stretching mode of the pyridinium cation and the coordinating cyanides, respectively. The low intensity signal of the cyanide stretches is due to their symmetry about the boron center and is typical of other tetracyanoborate species.[6,10] Characteristic absorptions due to the pyridine ring were also observed.

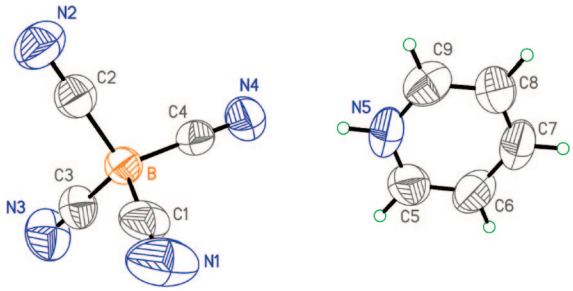

Figure 2. Structure of $[B(CN)_4]HNC_5H_5$. The heavy atoms are 50% probability ellipsoids, and the hydrogen atoms are of arbitrary size.

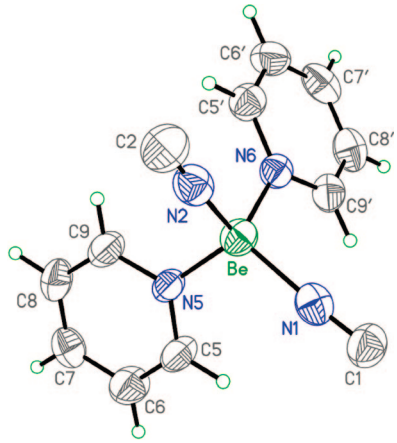

Figure 3. Structural representation of $Be(CN)_2(NC_5H_5)_2$.

The unexpected formation of this intriguing species prompted us to reexamine its synthesis with the objective to establish a pathway leading to pure compounds of this type via reactions involving HCN and $B(CN)_3NCSiMe_3$. Although the formation of $[B(CN)_4]HNC_5H_5$ (**2**) as a pure product remains elusive, our experiments demonstrate that such a simple compound which could readily deliver soluble $[B(CN)_4]^-$ species in organic media is within reach.

The successful synthesis of Lewis base compounds of $B(CN)_3$ described earlier prompted us to explore the formation of the coordination analogue $B(CN)_3NH_3$ via displacement reactions of $SiMe_3CN$ from $B(CN)_3NCSiMe_3$ using an excess of NH_3. Perhaps unexpected, a polycrystalline brittle solid was obtained and identified by IR spectroscopy and powder XRD to be the previously reported ammonium tetracyanoborate salt, $NH_4[B(CN)_4]$.[18] A possible pathway proceeds by analogy to "hydrolysis" of the Me_3SiCN ligand by NH_3 to produce Me_3SiNH_2 as described by eq 4.

$$B(CN)_3NCSiMe_3 + 2NH_3 \rightarrow Me_3SiNH_2 + NH_4[B(CN)_4] \quad (4)$$

Synthesis of Be and Ga Cyanide Adducts. The $Be(CN)_2(NC_5H_5)_2$ (**3**) adduct was simply formed by dissolving powder samples of the corresponding framework cyanide $Be(CN)_2$ in pyridine and heating the mixture at 110 °C. Pure and crystalline **3** is subsequently obtained (51% yield) by cooling the solution to –20 °C. The colorless air-sensitive solid sublimes under vacuum and melts sharply at 128 °C. The IR spectrum revealed a sharp absorption at 2112 cm^{-1}, characteristic of terminal C—N stretching modes, and the typical set of vibrational modes corresponding to the NC_5H_5 ring structure. A combustion analysis for C, H, and N of the bulk solid indicates a $Be(CN)_2(NC_5H_5)_2$ composition. A single-crystal XRD structural analysis confirms that the compound is a Lewis acid–base complex between two NC_5H_5 molecules and $Be(CN)_2$. This material crystallizes in space group $Pca2_1$ with four molecules in the unit cell. An ORTEP diagram showing the molecular conformation and the atom numbering scheme is presented in Figure 3. The Be central atom is four coordinate in a slightly disordered tetrahedral arrangement surrounded by two nitrogen and two carbon atoms of the pyridine rings and cyanide ligands, respectively. The average Be—N [1.753(4) Å] and Be—C [1.701(4)Å] bond distances are of reasonable value in comparison to those of the solid-state beryllium cyanide compound.[8] The C—N bond length [1.110(3) Å] also compares well with reported values.[17] The Be—C—N branches are nearly linear with corresponding angles of ~178°. The solid is noncentrosymmetric, and the absolute configuration could not be determined within any degree of certainty because of the absence of heavy elements in the structure. The direction in which either the pyridines or the cyanides were oriented with respect to the *c*-axis is unknown, but this is resolved below for similar systems using simulations. Nevertheless, in spite of a relatively large deviation in the Flack parameter, the observed *R*-factor of 3.9% is quite acceptable. The IR

(18) Küppers, T.; Bernhardt, E.; Willner, H.; Rohm, H. W.; Köckerling, M. *Inorg. Chem.* **2005**, *44*, 1015.

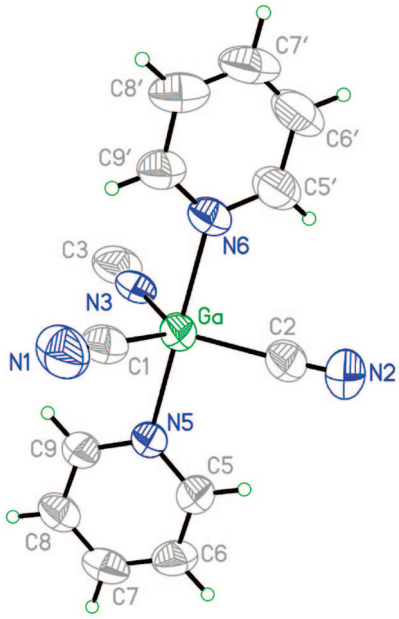

Figure 4. Structure of $Ga(CN)_3(NC_5H_5)_2$.

spectrum revealed a sharp absorption at 2112 cm^{-1}, characteristic of terminal C—N stretching modes, and the typical set of vibrational modes corresponding to the NC_5H_5 ring structure.

$Ga(CN)_3(NC_5H_5)_2$ (**4**) was obtained by dissolving powder samples of the $Ga(CN)_3$ framework in pyridine at room temperature. The excess pyridine was removed, and the resultant solid was recrystallized from a hot toluene solution to form colorless, air-sensitive crystals in 75% yield. A combustion analysis for C, H, and N is consistent with a $Ga(CN)_3(NC_5H_5)_2$ composition. A single-crystal XRD structure confirms that this compound is a Lewis acid–base complex between two NC_5H_5 solvent molecules and $Ga(CN)_3$. This material crystallizes in space group $P\bar{1}$ with two molecules per unit cell. An ORTEP diagram showing the molecular conformation and the atom numbering scheme is presented in Figure 4. The Ga center is pentacoordinate and exhibits a near perfect trigonal bipyramidal geometry. The two coordinating pyridines at the axial positions form nearly right angles in the range of 88.3−91.4° with respect to the three equatorial cyanides. The latter lie within the same horizontal plane and form NC—Ga—CN angles of 116.30(16), 121.19(15), and 122.46(15)°. The average Ga—N [2.194(3) Å] and Ga—C [1.991(4) Å] bond distances exhibit typical values in comparison to other gallium cyanide compounds.[4,19] However, the C—N bond length [1.075(5) Å] is significantly shorter than that found in the open-framework $Ga(CN)_3$ [1.148(1) Å] which is expected in view of the extended coordination of the cyanides in the latter. Selected bond lengths and angles of compound **4** are listed in Table 2. The IR spectrum revealed a sharp absorption band centered at 2180 cm^{-1} (C≡N stretch) and characteristic absorption bands due to pyridine coordination.

The similarity in structure and bonding properties between $Ga(CN)_3$ and $Al(CN)_3$ prompted efforts to prepare the Al molecular analogue of $Ga(CN)_3(NC_5H_5)_2$. Initial attempts to isolate the compound focused in dissolving $Al(CN)_3$ powder samples in dry pyridine. However, the highly robust cyanide framework was found to be completely insoluble and unreactive even under high temperature refluxing conditions. Further attempts involved a direct synthesis by metathesis of $AlCl_3$ with an excess of Me_3SiCN in pyridine. A white precipitate was obtained in this case after refluxing the mixture for several hours. Combustion analysis along with IR spectroscopy suggested that this material is a mixture of varying cyanide substitutions about the Al center. In contrast to $Al(CN)_3$, the $In(CN)_3$ framework dissolves readily in pyridine at room temperature. However, recrystallization of the resultant solid produced a combination of clusters and fibrous bundles, which were unsuitable for a reliable structural determination by XRD. Elemental analysis of the crystals indicated a mixture of products which may include $In(CN)_3(NC_5H_5)_2$ and $In(CN)_3(NC_5H_5)_3$. Therefore, the precise composition of these adducts could not be unambiguously determined. Motivated by this inhomogeneity and the differences in dissolution properties among the $Al(CN)_3$, $Ga(CN)_3$, and $In(CN)_3$ compounds and adduct stabilities, we next conducted a computational study which elucidates their origin. Most importantly these calculations uncovered important trends in the structures of the extended framework solids and those of the molecular compounds. The outcome of this inquiry and associated significant findings are described in the remainder of the paper.

Dissolution Energetics and Computational Details. In the context of understanding the dissolution behavior the formation of the molecules $M(CN)_3(NC_5H_5)_2$ from the corresponding $M(CN)_3$ solid frameworks are envisioned to occur in a pyridine environment via the idealized process described by eq 5:

$$M(CN)_3(s) + nNC_5H_5(sol) \rightarrow M(CN)_3(NC_5H_5)_n(sol) + \Delta H_n \quad (5)$$

where the intermediate step involving the dissolution of the solid framework to form solvated metal cyanide units denoted by "$M(CN)_3$"(sol) is not considered. Our strategy here is simply to compare the sum of the energies of the solid framework structure and the pyridine solvent to that of the molecular $M(CN)_3(NC_5H_5)_2$ product, as an estimate of the formation enthalpy ΔH_n in the above equation. To obtain these energies, which are needed in eq 5 to explain solubility trends, detailed electronic structure calculations were carried out for the $M(CN)_3$ solids (M = Al, Ga, In) as well as for the corresponding $M(CN)_3(NC_5H_5)_2$ and NC_5H_5 molecular species to determine the equilibrium structures and energies. However, it should be noted that mono- and tripyridine derivatives in the $M(CN)_3(NC_5H_5)_n$ class where n = 1–3 may also form in these solutions (see Figure 5), and we therefore also consider their formation in our simulations. One objective in this regard is to investigate the role of steric interactions in the stability of these various molecular derivatives relative to the framework solid analogues with the aim of providing an explanation for the absence of pure and crystalline $M(CN)_3(NC_5H_5)_2$ (M = Al and In) in our reaction products.

(19) Uhl, W.; Hannemann, F. *Eur. J. Inorg. Chem.* **1999**, *201*, 207.

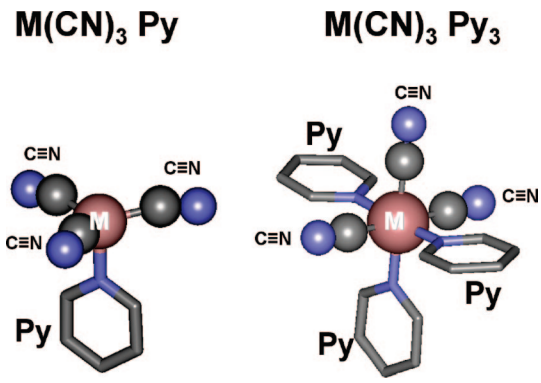

Figure 5. Structure predicted for the hypothetical monopyridine $M(CN)_3(NC_5N_5)$ and tripyridine $M(CN)_3(NC_5H_5)_3$ molecules (Py = NC_5N_5).

To ensure consistency in the energetic comparisons, the extended framework solids and molecular forms were simulated using the same approximations and methodology. The computational details are as follows: We used density functional theory in the local density approximation (LDA) to obtain the electronic structure *for all molecules and solids*, in spite of its well-known tendency to overestimate binding energies and underestimate bond lengths. All systems were represented in a periodic setting using the projected augmented wave (PAW) electronic structure approach,[20] as implemented in the VASP code.[21] (Note: the application of more quantitative model chemistries based on the B3LYP functional requires a systematic treatment of electronic structure of both molecules and solids, which is currently not available in VASP.) The following valence configurations were used in our treatment, $H[1s^2]$, $C[2s^22p^2]$, $N[2s^22p^3]$, $Al[3s^23p^1]$, $Ga[4s^23d^{10}4p^1]$, and $In[5s^24d^{10}5p^1]$, and an energy cutoff of 800 eV (1 eV = 96.485 kJ/mol) was used to generate electronic states in plane waves. The molecules were placed within large 16 × 16 × 16 $Å^3$ cubic cells to ensure negligible interactions between molecules, and a single *k*-point was used to sample the Brillouin zone. For the periodic framework solids a much denser 8 × 8 × 8 Monkhorst–Pack grid[22] was used to generate 60 irreducible *k*-points for reciprocal space integration. Using these computational conditions the equilibrium static-lattice structure of the $M(CN)_3$ materials was obtained by simultaneously optimizing the cell shape, cell volume, and internal atomic positions to a convergence of better than 0.002 eV/Å for the atomic forces and 0.1 kB for the external stress. In the case of the molecular systems the supercell parameters were held fixed while all atomic positions were optimized to an accuracy of 0.001 eV/Å.

The computational results of the ground-state electronic energies for $M(CN)_3$, $M(CN)_3(NC_5H_5)_n$, and pure NC_5H_5 are summarized in Table 3, along with the value for ΔH_n corresponding to the process described in eq 5. A graphical representation of these results is also provided in Figure 6. It should be noted that the total energies generated by the VASP code, as listed in Table 3, are referenced to the sum of the spin-averaged atomic constituent energies. Vibrational entropy contributions are not likely to alter these predicted trends because the basic structures of the solids and molecules involved in each of the comparisons are the same. Similarly, the neglect of solvation energy is also likely to produce a small constant shift in the energy differences across the sequence because the structures of the intermediate compounds, such as the solvated "$M(CN)_3$" cores, are nearly identical.

The generic calculated structures of the $M(CN)_3(NC_5H_5)_n$ (n = 1, 3) adducts are shown in Figure 5. The mono adducts of Al, Ga, and In all form pseudotetrahedral structures in which the bond angles approach the ideal value as the size of the central metal increases. The triadducts exhibit ground-state structures comprised of octahedrally coordinated metals centers surrounded by pyridine rings which are aligned along the octahedral axes, indicating minimal steric hindrance. The diadducts are described in greater detail below, and their structural parameters are compared with experimental molecular and solid-state analogues.

According to our simulations all $Al(CN)_3(NC_5H_5)_n$ (n = 1–3) adducts are predicted to be metastable with respect to $Al(CN)_3$ and pyridine. The dashed lines in Figure 6 represent the "energy landscape" between the various compounds and reflect the reasonable assumption that the reaction to form all diadducts from their monoadduct counterparts is barrierless. In the case of the gallium compounds the data show that the $Ga(CN)_3(NC_5H_5)_n$ (n = 2–3) are predicted to be energetically stable. However, the formation of the tripyridine form is likely suppressed by a significant kinetic barrier. Among the indium compounds the $In(CN)_3(NC_5H_5)_n$ (n = 1–2) derivatives appear to be thermodynamically unstable. The $In(CN)_3(NC_5H_5)_3$ species, however, is predicted to have zero enthalpy of formation and differs in energy by only 21 kJ/mol from its $In(CN)_3(NC_5H_5)_2$ counterpart. This small difference, in combination with a smaller kinetic barrier between di- to tri-adducts (accommodated by the large In center) may explain the formation of adduct mixtures in our experiments as evidenced by the elemental analysis data. The calculation of transition states between the various adducts, as well as a comparative study of the energetics using other model chemistries, will be addressed in future work. Collectively these data are consistent with the experimental results which show that the Ga compound is readily isolated in pure crystalline form.

Correlations between $M(CN)_3$ Solids and $M(CN)_3(NC_5H_5)_2$ Molecular Analogues. A valuable byproduct of extended calculations of the type described above yielded the ground-state structures of the extended framework solids and those of the molecular compounds. The calculated structural parameters obtained here can then be compared directly with experimental values determined by XRD studies on both solid-state and molecular systems including $Ga(CN)_3(NC_5H_5)_2$. As we demonstrate below our simulations yield new information about these materials and elucidate subtle structural trends that may have significance for their practical use. For instance, the $M(CN)_3$ class of framework compounds considered here affords potential opportunities

(20) Blöchl, P. E. *Phys. Rev. B* **1994**, *50*, 17953.
(21) Furthmüller, J.; Cappellini, G.; Weissker, H. C.; Bechstedt, F. *Phys. Rev. B* **2002**, *66*, 45110.
(22) Monkhorst, H. J.; Pack, J. D. *Phys. Rev. B* **1976**, *13*, 5188.

Table 3. Calculated Electronic Energies (in eV) of $M(CN)_3$, NC_5H_5, and $M(CN)_3(NC_5H_5)_n$, for n = 1–3 [a]

M	$M(CN)_3$(solid)	(NC_5H_5)	$M(CN)_3(NC_5H_5)$	ΔH_1	$M(CN)_3(NC_5H_5)_2$	ΔH_2	$M(CN)_3(NC_5H_5)_3$	ΔH_3
Al	−60.760	−75.805	−134.066	+241	−211.260	+107	−288.009	+16
Ga	−57.526	−75.805	−132.440	+86	−209.181	−4	−285.325	−37
In	−56.552	−75.805	−131.052	+126	−207.941	+21	−283.958	0

[a] Also listed are the corresponding reaction enthalpies ΔH_n (in kJ/mol), which are obtained as the electronic energy difference for the process shown in eq 5.

in topical and emerging technological areas such as hydrogen storage for renewable energy and negative thermal expansion (NTE) applications. The structural data derived here indicates that the M—CN—M linkages become progressively noncollinear along the $Al(CN)_3$ to $In(CN)_3$ series which may explain the minor unresolved splitting in the high index XRD peaks of the $Ga(CN)_3$ reported by Williams et al.[7] Such deviations from linearity have recently been identified as the mechanistic origin for NTE behavior in related Prussian blue and transition metals analogues[3] suggesting that the $In(CN)_3$ species may be of particular interest for NTE because it exhibits remarkably large M—CN—M noncollinearity. For hydrogen storage applications the key design parameters are pore volume and chemical activity at absorption sites within the framework. To our knowledge $M(CN)_3$ frameworks represent the simplest class of materials exhibiting a large lattice parameter range, with $In(CN)_3$ in particular exhibiting one of the largest pore volumes (179 $Å^3$ per formula unit) among Prussian blue compounds. Continuous solid solutions can be readily formed by alloying the metal sites allowing for simultaneous tuning of both pore volume and site reactivity.

Properties of $M(CN)_3$ Framework Solids. In prior work we synthesized the $Al(CN)_3$, $Ga(CN)_3$, and $In(CN)_3$ compounds and showed for the first time that they crystallize in a classic "Prussian blue"-like octahedral network.[4,5,8] As shown in Figure 7, the M ions occupy the corners of the cubic lattice while the C≡N units lie along the edges of the simple cubic unit cell. Rietveld refinement indicated that the cyanides are orientationally disordered, with an average of three N and three C coordinating to a metal site.

In the present study we have adopted a simplified description based on a primitive cell containing one $M(CN)_3$ formula unit, in which the C—N linkages are ordered as shown in Figure 7. Table 4 compares our calculated structures with those measured experimentally for $Al(CN)_3$, $Ga(CN)_3$ and $In(CN)_3$. The simulated parameters are in fairly good agreement with their observed counterparts except the C—N bond distances. For example, the lattice constants are underestimated systematically by ∼1% which is typical for the LDA treatment. The C≡N bond distances predicted by LDA remain essentially constant with value of 1.157 Å, as expected based on the enormous stiffness of the C≡N triple bond. In the case of $Al(CN)_3$ the calculated C≡N distance (1.158 Å) is slightly lower than that observed (1.164 Å) by an amount consistent with the LDA underestimate, as expected. Furthermore these particular values are essentially identical within the reported XRD standard deviation. By contrast the experimental C≡N bond distances decrease systematically in value from 1.164 Å for $Al(CN)_3$ to 1.125 Å for the $In(CN)_3$ which corresponds to a 3.5% change. The largest deviation in C≡N bond distances between the LDA estimates and the experimental values (+2.8%) is observed for $In(CN)_3$. We note that for this case LDA predicts the largest departure from colinearity in the In—CN—In linkage. This suggests that the neglect of this subtle affect in the X-ray refinement of the structure might have led to an underestimate of the true C≡N bond distance. A schematic illustrating the calculated deviations from colinearity in M—C≡N—M for Al, Ga, and In compounds is shown in Figure 8. Note the maximum deviation occurs in the In—C≡N—In linkage for which the experiments show the shortest C—N bond distance.

Also listed in the Table 4 are the individual bond lengths from the metal site to both the nitrogen (M—N) and carbon (M—C) in the cyanide unit. From simulation it is found that the deviation of these from their mutual average, ⟨M—(C,N)⟩, is ∼0.05, 0.01, and 0.04 Å in $Al(CN)_3$, $Ga(CN)_3$, and $In(CN)_3$, respectively. These small deviations may be associated with the CN ordering in our model and could average out in an orientationally disordered solid. To explore this possibility we carried out a single large-scale control calculation on an orientationally disordered model of In-

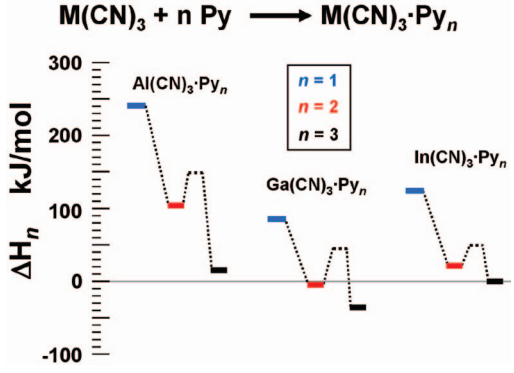

Figure 6. Graphical representation of the formation enthalpies provided in Table 3 for the reaction $M(CN)_3 + nPy \rightarrow M(CN)_3Py_n$ (Py = NC_5N_5).

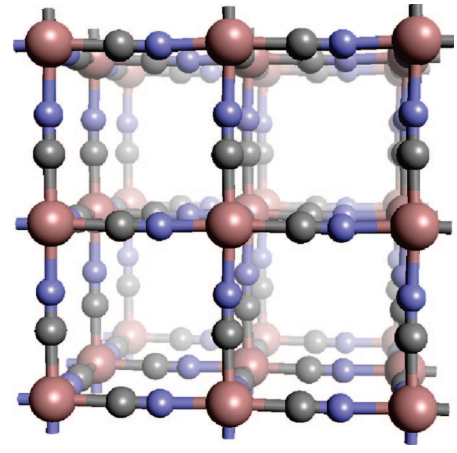

Figure 7. Idealized ordered structure of the $M(CN)_3$ framework solid used in the calculations.

Table 4. Comparison of the Calculated and Observed Structural Parameters for the $Al(CN)_3$, $Ga(CN)_3$, and $In(CN)_3$ Framework Compounds[a]

	$Al(CN)_3$	% error	$Ga(CN)_3$	% error	$In(CN)_3$	% error
C—N	1.158 (1.164)	−0.6	1.156 (1.148)	+0.9	1.157 (1.125)	+2.8
M—C	2.050		2.037		2.189	
M—N	1.941		2.055		2.271	
⟨M—(C,N)⟩	1.996 (2.021)	–1.2	2.046(2.072)	–1.3	2.230 (2.251)	–0.9
$\sum b$	5.149 (5.190)	–0.8	5.248 (5.292)	–0.8	5.617(5.627)	–0.2
a	5.148 (5.205)	–1.1	5.244 (5.295)	–1.0	5.603(5.627)	–0.4

[a] Experimental values are listed in parentheses, and all lengths are reported in Å. Also listed is $\sum b$, the simple sum of the M—C, C—N, and N—M bond lengths, and the lattice parameter, a.

$(CN)_3$, in which the deviations are expected to be the largest in magnitude. The system was represented by a $3 \times 3 \times 3$ supercell with stoichiometry $In_{27}(CN)_{81}$ in which the CN units were randomly oriented (the converged structure is shown in Figure 9). A second calculation using the ordered model was also carried out in the same supercell setting for comparison. To make the calculations tractable we replaced the PAW potentials by ultrasoft LDA pseudopotentials, which are based on simpler $In[5s^25p^1]$ valence configurations. An energy cutoff of 600 eV was used in the plane wave expansion and a single k-point at Γ was used to sample the Brillouin zone. Both the ordered and the random supercells remained approximately cubic in symmetry and converged to the same lattice parameter, ∼5.577 Å (slightly shorter than PAW result for the ordered $In(CN)_3$ of 5.603 Å). With regards to thermodynamic stability we find that the ordered supercell is 0.569 eV lower in energy than the orientationally disordered model. This energy difference corresponds to 0.7 kJ/mol per CN unit, or ∼2 kJ/mol per formula unit, and indicates that the order/disorder in framework cyanides is dominated by configurational entropy, $\Delta S_{conf} = 3R \ln 2$ per formula unit (at room temperature $T\Delta S_{conf} \sim 5$ kJ/mol).

Our orientationally disordered model also provides access to new information concerning the bond length and bond angle distributions in the framework structures (Figure 9). The simulations indicate that a very narrow distribution of CN bond lengths, centered on 1.156 ± 0.001 Å, is maintained in spite of significant noncollinearity, as manifested in the fairly wide distribution of M—CN angles ($\sim 177 \pm 2°$). This is consistent with the incredible rigidity of the triple CN bond. In contrast, the softer In—N and In—C bonds exhibit a much wider bond length distribution, centered at 2.20 ± 0.05 Å and 2.23 ± 0.04 Å, respectively (note: the corresponding values in the ordered lattice were close at 2.19 Å and 2.27 Å, respectively). These results are thus generally consistent with the corresponding deviations found in the simple ordered model, indicating that noncollinearity of the CN units is a general model-independent feature of $M(CN)_3$ framework solids. The overall agreement between the simulated and the observed data is gratifyin and suggests that the approach employed affords excellent predictive capability.

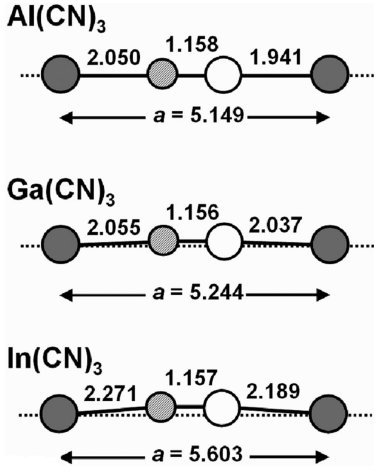

Figure 8. Graphical representation of the M—C≡N—M unit noncollinearity in the $Al(CN)_3$, $Ga(CN)_3$, and $In(CN)_3$ framework compounds (metal atoms, dark grey; N, light grey, C, white). Calculated LDA bond lengths and unit cell edge lengths, a, are listed in Å. The differences between the lattice parameter and sum of the bond lengths are $\Delta b = 0.001$, 0.004, and 0.014 Å for $Al(CN)_3$, $Ga(CN)_3$, and $In(CN)_3$, respectively.

Properties of $M(CN)_3(NC_5H_5)_2$ Molecules. The experimental structure determination of the $Ga(CN)_3(NC_5H_5)_2$ molecule shows that two of the C—N bonds lengths are equal (1.075 Å) while the third is anomalously short (1.019 Å). All of these values are in fact significantly shorter than those observed in the framework solids and other molecular systems incorporating terminal CN ligands. Nevertheless the speciation of two long and one short bond has in fact been reported in a recent structural determination of the mesityl-$Ga(CN)_3$ anion in the $Et_4N[mesGa(CN)_3]$ salt where the C—N bond lengths are found to be 1.139 Å, 1.130 Å, and 1.074 Å.[23] Note that the shortest of these (1.074 Å) is close to the longest C—N bond distance (1.074 Å) observed in our $Ga(CN)_3(NC_5H_5)_2$ structure. Collectively these large variations in terminal C—N bond lengths prompted us to undertake a brief computational study of all three possible pyridine adducts $M(CN)_3(NC_5H_5)_2$ to elucidate the origin of the C—N bond distributions. In addition to providing an explicit comparison between theory and experiment for the synthesized $Ga(CN)_3(NC_5H_5)_2$ molecule this simulation study also provides insight into trends throughout the entire $M(CN)_3(NC_5H_5)_2$ sequence. Finally, the bonding and electronic structure of the extended $M(CN)_3$ framework solids and that of their $M(CN)_3(NC_5H_5)_2$ molecular analogues can be systematically compared.

Tables 5 and 6 provide a summary of the calculated structure of $Ga(CN)_3(NC_5H_5)_2$, including unit cell parameters and intramolecular bond lengths and angles. Using the structures of the isolated molecules as a starting point we simultaneously optimized the unit cell volume and shape and all atomic positions without any symmetry assumptions until the residual forces were below 0.001 eV/Å. The LDA

(23) Yao, H.; Kuhlman, M. L.; Rauchfuss, T. B.; Wilson, S. R. *Inorg. Chem.* **2005**, 44.

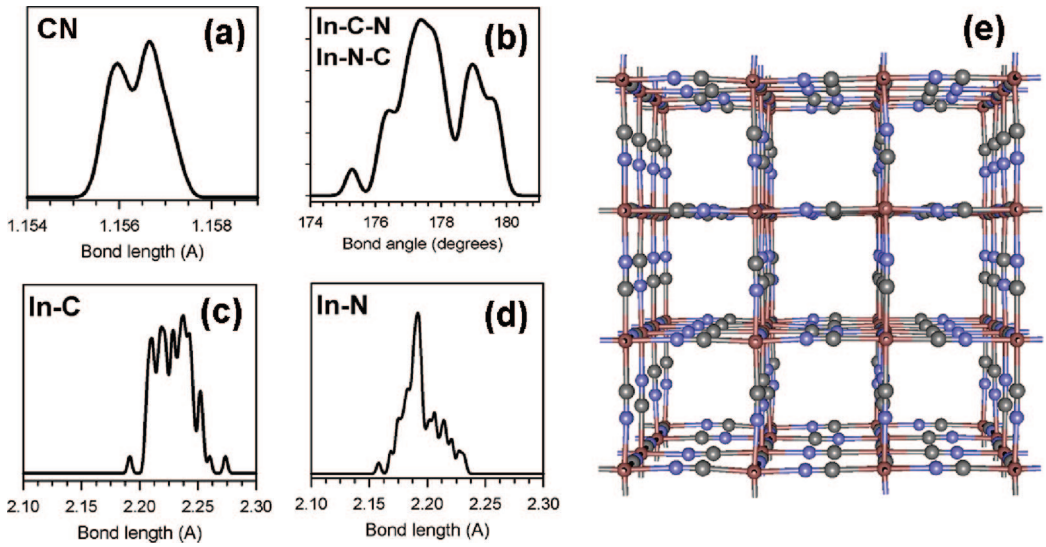

Figure 9. CN bond length (a) and In—CN bond angle (b) distributions in an orientationally disordered 3 × 3 × 3 supercell representation of $In(CN)_3$. The In—C and In—N bond length distributions are shown in parts c and d, respectively. The structurally optimized atomic configuration obtained from our simulations with mean edge length $a = 5.577$ Å is shown in part e.

Table 5. Comparison of Simulated LDA and Observed Cell Parameters for the Crystallized Molecular $Ga(CN)_3(NC_5H_5)_2$ Compound (Triclinic Space Group $P\bar{1}$)

	observed	LDA	difference
a (Å)	7.558	7.209	–5.3%
b (Å)	8.286	7.882	–5.5%
c (Å)	12.763	11.638	–8.4%
α (Å)	77.809	75.89	–2.5%
β (Å)	75.389	79.09	+4.7%
γ (Å)	71.894	68.29	–5.0%

Table 6. Comparison of the Calculated and Observed Structural Parameters for the $Ga(CN)_3(NC_5H_5)_2$ Molecule. Bond Lengths and Bond Angles Are Listed in Å and Degrees, Respectively

molecular core	observed	LDA	% dev
	Bond Lengths (Å)		
Ga—C1	2.017	1.934	–4.3
Ga—C2	2.000	1.948	–2.7
Ga—C3	2.063	1.956	–5.4
Ga—N5	2.170	2.101	–3.2
Ga—N6	2.218	2.124	–4.2
C1—N1	1.076	1.161	7.3
C2—N2	1.077	1.161	7.3
C3—N3	1.043	1.161	10.2
	Bond Angles (deg)		
Ga—C1—N1	179.6	179.6	0.0
Ga—C2—N2	176.9	177.3	–0.2
Ga—C3—N3	178.6	177.3	0.7
N5—Ga—N6	178.0	178.8	0.4
C1—Ga—N5	90.76	90.6	–0.2
C2—Ga—N5	91.47	92.5	1.2
C3—Ga—N5	89.98	90.0	0.0
C1—Ga—N6	88.59	90.9	2.5
C2—Ga—N6	90.94	88.6	–2.6
C3—Ga—N6	88.32	88.3	0.0

treatment yields an underestimate of the unit cell dimensions on the order of 5–8%, which is greater than the typical 1–2% obtained in the case of close packed solids (Table 5). For molecular crystals, such as the present example, the LDA does not account for the long-range nature of the polarization forces. Nevertheless the LDA yields the correct lattice symmetry (monoclinic) with typical bond angle deviations on the order of −3–5%. Table 6 describes the bond lengths and bond angles of the "$Ga(CN)_3$" core and corresponding axial bonds to the pyridine units (note, the atomic labeling follows that defined in Figure 4). The observed and calculated bond lengths and angles within the pyridine units are within ∼0.5–1.0%, and we therefore do not discuss them in detail here. Briefly, the C_5N rings are planar (all torsion angles 180 ± 0.1°) and contain two symmetrical C—N bonds at 1.33 Å, two nearly parallel C—C bonds at 1.38 Å, and two apical C—C bonds with bond length ∼1.36 Å. The calculated C—H bonds lengths are all ∼1.10 Å. The calculated Ga—(C≡N) bonds are within normal range and agree fairly well (within 2–3%) with the experimental values. The calculated C≡N bond distances are essentially identical (1.16 Å) in contrast to the observed values (1.076 Å, 1.077 Å,and 1.043 Å). We have verified that the residual quantum mechanical forces on these atoms are vanishingly small, confirming a high degree of optimization. The large non-bonded distances between the terminal C≡N and the neighboring molecules preclude any effects associated with crystal packing. We therefore attribute the anomalously large deviation between the LDA and the observed values (8–12%) to refinement artifacts associated with the small scattering factors of C and N.

Table 7 lists the calculated bond lengths and bond angles of the molecular cores across the entire $M(CN)_3(NC_5H_5)_2$ sequence (M = Al, Ga, In). The calculated C≡N bond distances are essentially identical (1.16 Å) in all three compounds and agree closely with those calculated for the framework solid-state systems (1.16 Å). The M—C and M—N bond lengths are very similar in both the Al and the Ga compounds but increase significantly in the In case. In general the average M—(C,N) distances in the molecules (Table 7) and solids (Table 4) agree to within 0.03 Å confirming that the calculations are internally consistent and that the bond trends of the molecular cores are conferred to the corresponding solids.

Table 7. Comparison of the LDA Structural Parameters for the $M(CN)_3(NC_5H_5)_2$ Molecules (M=Al,Ga,In). The Labeling of the Atom Positions Follows the Structural Model in Figure 4. Bond Lengths and Bond Angles are Listed in Å and Degrees, Respectively

	Al	Ga	In
	Bond Lengths (Å)		
M—C1	1.959	1.934	2.122
M—C2	1.961	1.948	2.129
M—C3	1.961	1.956	2.129
M—N5	2.084	2.167	2.219
M—N6	2.087	2.168	2.218
C1—N1	1.162	1.160	1.161
C2—N2	1.162	1.160	1.161
C3—N3	1.161	1.160	1.160
	Bond Angles (deg)		
M—C1—N1	175.8	177.3	176.4
M—C2—N2	179.1	179.6	179.5
M—C3—N3	176.9	177.3	176.7
N5—M—N6	179.8	178.8	179.0

Electronic Structure. The converged electronic wave functions, charge density, and potential also yield the electronic band structure for the framework solids. All three $M(CN)_3$ compounds are predicted to be insulators, and a representative plot of the bands is shown for $Ga(CN)_3$ in Figure 10. The valence and conduction band structure is very similar for $Al(CN)_3$ and $In(CN)_3$, exhibiting direct gaps at the Γ point. The LDA band gaps are calculated to be 4.8, 4.9, and 5.2 eV for $Al(CN)_3$, $Ga(CN)_3$, and $In(CN)_3$, respectively. A well-known shortcoming of the LDA is that the band gaps are typically underestimated by a factor of 2, in spite of the excellent predictive capability of the LDA with regard to cohesive and structural trends. The experimental band gap values are therefore expected to lie within the range of ∼8–10 eV. The electronic structure of the $Ga(CN)_3(NC_5H_5)_2$ molecule is compared with that of its framework analogue $Ga(CN)_3$ in Figure 11. Both systems were treated using the LDA and identical pseudopotentials, and computational parameters were employed. These LDA calculations reveal that the highest occupied molecular orbital–lowest unoccupied molecular orbital gap in the molecular core systems is similar in magnitude to the band gap in the solids. We note that energy levels correspond to orbitals which extend throughout the molecular structure. The close "molecules to solids" correspondence of the electronic structure is remarkable in view of the large difference in bonding geometries between the two materials, namely, 5-fold bipyramidal in the molecules and corner shared octahedral in the solids.

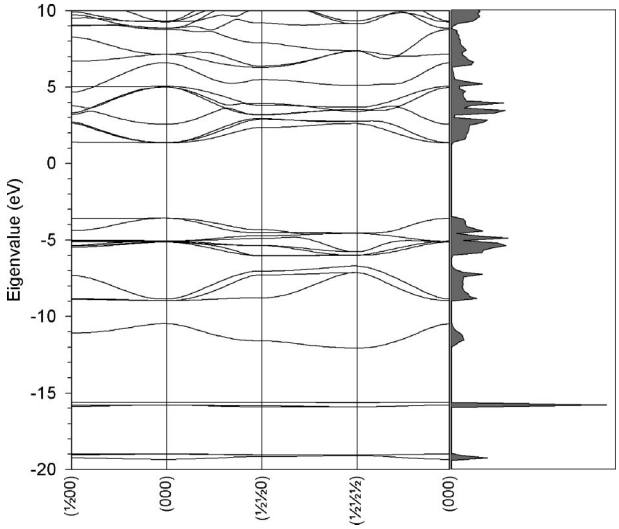

Figure 10. Band structure and density of states of the $Ga(CN)_3$ framework solid.

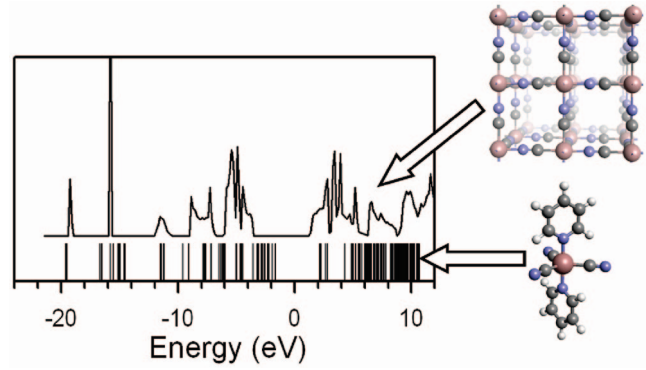

Figure 11. Correspondence between the calculated electronic density of the $Ga(CN)_3$ and the molecular orbital level spectrum of the $Ga(CN)_3(NC_5H_5)_2$ molecule.

Conclusions

We have conducted an experimental study involving synthesis and structural elucidations of the molecular adducts $B(CN)_3NC_5H_5$ (**1**), $[B(CN)_4]HNC_5H_5$ (**2**), $Be(CN)_2(NC_5H_5)_2$ (**3**), and $Ga(CN)_3(NC_5H_5)_2$ (**4**). A detailed theoretical treatment of dissolution energetics showed that crystal growth for the latter compound is readily achieved because of its greater stability relative to the Al and In counterparts. The optimized framework structures obtained form these simulations for the ordered cyanide lattices revealed slight but systematic noncollinearities in the M—CN—M linkages along the Al, Ga, and In tricyanide sequence. This result could explain the anomalous short cyanide bond lengths deduced previously by powder XRD analysis of the solids. To verify this findings we carried out large scale simulations on orientationally disordered nanoscale representations of the $In(CN)_3$ species where such deviations are expected to be the largest. The results confirm the noncollinearity found in the simple ordered models and demonstrated that the order/disorder difference between cyanides in the Prussian Blue structure is very small (∼2 kJ/mol per formula unit). In this context our results also indicate that canonical orientational disorder described in prior extensive XRD or neutron scattering studies is likely due to configurational entropy. Finally we compared the experimental structure for the molecular crystal $Ga(CN)_3(NC_5H_5)_2$ with its simulated LDA structure and found good agreement with the exception of the terminal C—N bond lengths which were equal in the simulated structures and significantly speciated in the crystal data. Isolated $M(CN)_3(NC_5H_5)_2$ molecules were also simulated, and the resulting structural data followed closely the corresponding trends in the framework solid analogues. This was also found to be the case for the electronic structure in which the molecular orbital energies for the $M(CN)_3$ molecular cores exhibited a close correspondence with density of states features in the solids.

Table 8. Fraction of Isocyanide Determined in the CN Groups in 1, 2, 3, and 4

isocyanide fraction	$B(CN)_3NC_5H_5$	$[B(CN)_4]HNC_5H_5$	$Be(CN)_2(NC_5H_5)_2$	$Ga(CN)_3(NC_5H_5)_2$
C1—N1	0.06(2)	0.05(3)	0.67(4)	0.44(5)
C2—N2	0.06(3)	0.06(3)	0.57(5)	0.23(5)
C3—N3	0.04(2)	0.07(3)		0.78(6)
C4—N4		0.01(3)		

Experimental Section

General Considerations. Reactions were performed under prepurified nitrogen using standard Schlenk and drybox techniques. Dry, air-free solvents were distilled from either sodium benzophenone ketyl or P_2O_5 under nitrogen prior to use. Fourier transform infrared spectra were recorded on a Nicolet-Magna IR 550 spectrometer as a Nujol mull between KBr plates. The ^{13}C NMR spectra were collected on a Varian INOVA 500 MHz spectrometer, and the data were referenced to the $CDCl_3$ solvent signal of 77.16 ppm. A relaxation delay of 60 s was used for compound **3** and 10 s for compound **4**. Elemental analyses were performed by Desert Analytics (Tucson, AZ). Me_3SiCN (Gelest, 95%) was purified by trap-to-trap distillation prior to use. $BeCl_2$ (Alfa, 99%), BF_3 (Air Liquide, 99.5%), $GaCl_3$, and $InCl_3$ (Aldrich, 99%) were used as received. **Caution:** Manipulations involving cyanides should be performed in a well-ventilated hood and handled with the utmost care.

$B(CN)_3NCSiMe_3$. BF_3 (0.7 g, 0.010 mol) was condensed into a 100 mL Schlenk flask, containing an excess of Me_3SiCN (6.5 g, 0.066 mol) at –196 °C. The flask was warmed slowly to 25 °C, and the solution was stirred for ~12 h, upon which a brown slurry developed. The volatiles were removed in vacuum, and additional Me_3SiCN (1.0 g, 0.010 mol) was added directly to the solid. The mixture was heated at 70 °C for 18 h after which it was cooled and filtered. The resultant solid was washed with hexane and dried in vacuum to produce near quantitative yields of the compound which was characterized by IR spectroscopy and powder XRD. The characterization data including IR and NMR results are given in ref 6.

$B(CN)_3NC_5H_5$ (1) and $[B(CN)_4]HNC_5H_5$ (2). A 200 mL Shlenk flask was charged with 1.0 g of crude (unsublimed) $B(CN)_3 \cdot NCSiMe_3$, and 30–35 mL of pyridine was added via canulation (the pyridine was dried over sodium/benzophenone ketyl for at least 8 h and further dried over molecular sieves for 18 h at room temperature). The dark solution was heated at 75 °C for 24 h, after which the volatiles were removed in vacuum leaving an oily dark solid. The product was extracted with chloroform which formed a clear, amber-colored solution. The solution was reduced and placed in a freezer (–20 °C). Colorless platelets were obtained after a few days. Repeated concentration and cooling of the solution produced several crops of crystals to give an overall yield of 0.340 g (~40% yield). The crystalline solid was found to be predominantly $B(CN)_3NC_5H_5$ (**1**) with a small amount of impurity comprised of single-crystalline $[B(CN)_4]HNC_5H_5$ (**2**). The latter was easily separated from **1** on the basis of crystal morphology and appearance. A combustion analysis of **1** is in good agreement with the calculated composition. Calcd: C, 57.2%; N, 33.4%; H, 3.0%. Found: C, 56.92%; N, 33.06%; H, 2.82%. Mp = 170 °C. IR (Nujol, cm^{-1}): 3123 (m), 3070 (m), 2227 (m), 1633 (s), 1495 (s, sh), 1226 (m), 1165 (m), 1132 (s), 1029 (m), 975 (s), 938 (s), 897 (m), 871 (s), 770 (s), 681 (s) 656 (w), 510 (w), 433 (w), 389 (w). IR of **2** (Nujol, cm^{-1}): 3244 (m), 3174 (m), 3078 (m), 2229 (w), 1637 (m), 1617 (s), 1543 (s), 1484 (s), 1253 (w), 1055 (m), 933 (s), 750 (s), 681 (s), 612 (w), 496 (m).

Reaction of $B(CN)_3NCSiMe_3$ with NH_3. A 50 mL Schlenk flask was charged with (0.250 g, 1.3 mmol) $B(CN)_3NCSiMe_3$ and an excess of ammonia (800 L·Torr; 48 mmol) was condensed into the flask at –196 °C. The flask was pressurized with an atmosphere of nitrogen and slowly warmed to room temperature with the container open to the mercury bubbler, allowing any overpressure of ammonia to escape. A dark-brown slurry developed immediately and was stirred for 30 min. Afterward, the volatiles were removed in vacuum leaving behind a dark, crystalline, and brittle solid (0.128 g; yield = 91%) that was washed with 40 mL of hexane. IR spectroscopy and powder XRD analysis indicated the formation of $NH_4[B(CN)_4]$ reported elsewhere.

$Be(CN)_2(NC_5H_5)_2$ (3). A 50 mL flask was charged with a with 0.140 g of $Be(CN)_2$ and 20 mL of dry pyridine. The mixture was heated at 110 °C for 3 h, upon which the $Be(CN)_2$ dissolved completely. The clear-yellow solution was cooled to –20 °C to yield colorless blocky crystals, one of which was used to conduct a crystallographic study. An overall yield of ~51% was obtained by successive concentration and cooling of the solution. Mp = 128 °C. IR (Nujol, cm^{-1}): 2112 (s), 1616 (s) 1575 (w), 1492 (m), 1246 (w), 1219 (m), 1156 (w), 1074 (s), 1057 (s), 1021 (m), 810 (m), 790 (m), 759 (m), 727 (s, br), 699 (s, br), 650 (w), 619 (m), 600 (w), 572 (s), 554 (w), 448 (w). ^{13}C NMR ($CDCl_3$): δ 123.87 (s), 136.1 (s), 150.00 (s) (pyridine carbons) and δ 188.32 (s) (CN carbon). Anal. Calcd for $BeC_{12}N_4H_{10}$: C, 65.76; H, 4.56; N, 25.56. Found: C, 65.58; H, 4.56; N, 25.26.

$Ga(CN)_3(NC_5H_5)_2$ (4). A 50 mL Schlenk flask was charged with 0.310 g of $Ga(CN)_3$ and 15 mL of dry pyridine. The $Ga(CN)_3$ dissolved completely in pyridine, and the excess solvent was subsequently removed in vacuum to yield a microcrystalline colorless solid. This was dissolved in hot toluene at 75 °C, allowed to cool to room temperature, and recrystallized in a freezer at –20 °C to yield transparent blocky crystals after several days. Concentration and cooling of the solution produced several crops of these crystals to give an overall yield of ~75%. A suitable specimen was used to conduct a crystallographic study of the compound. Mp = 143 °C. IR (Nujol, cm^{-1}): 3117 (w), 3068 (w), 2180 (m), 1608 (s), 1490 (s), 1217 (s), 1157 (w, br), 1066 (s), 1042 (s), 1011 (s), 765 (s), 699 (s), 632 (s), 436 (s), 371 (s). ^{13}C NMR ($CDCl_3$): δ 125.75 (s), 139.98 (s), 146.67 (s) (pyridine carbons) and δ 128.14 (s) (CN carbon). Anal. Calcd for $GaC_{13}N_5H_{10}$: C, 51.04; H, 3.27; N, 22.90. Found: C, 49.99; H, 3.21; N, 21.56.

Structural Determination of 1, 2, 3, and 4. Colorless and pale yellow crystals of $B(CN)_3NC_5H_5$ (**1**) (0.377 × 0.282 × 0.036) mm^3 and $[B(CN)_4]HNC_5H_5$ (**2**) (0.320 × 0.190 × 0.0800) mm^3, respectively, were mounted in 0.3 mm glass capillary tubes for data collection utilizing a Bruker SMART APEX diffractometer. In the case of **2**, all six hydrogens on the pyridinium cation were clearly visible in the difference map near the final stages of refinement. The hydrogens were placed using geometrical considerations and allowed to refine as riding atoms on their bonding partners. Similarly the structures of $Ga(CN)_3(NC_5H_5)_2$ (**4**) and $Be(CN)_2(NC_5H_5)_2$ (**3**) were determined using crystals with size (0.375 × 0.250 × 0.200) mm^3 and (0.370 × 0.220 × 0.170) mm^3, respectively. These were mounted inside a 0.3 mm glass capillary tube and sealed under nitrogen. The latter compound adopts an acentric space group $Pca2_1$. Although attempts were made to determine the absolute configuration, there is a high degree of uncertainty in the Flack parameter because there are no heavy atoms in the structure. In all four structures, the possibility of cyanide/isocyanide disorder was

determined by creating cyanide/isocyanide pairs that were constrained to a total pair occupancy of 1.00, with further constraints that equivalent atomic coordinates and thermal parameters were maintained for each (partial C/partial N) at each atomic site. These disordered pairs were then allowed to refine to the fraction of cyanide and isocyanide at each particular (M—CN/M—NC) site. As shown in Table 8, the compounds with boron centers have virtually no isocyanide. The beryllium and gallium compounds have significant isocyanide at each (M—CN/M—NC) site, although there is no readily apparent reason for the variation of cyanide/isocyanide fraction among the sites within each compound. It should be noted that refinements with only ordered cyanide were initially performed on all four compounds. However, upon submission of the resulting CIF files to the *checkCIF* utility provided on the www.IUCr.org Web site, unacceptable Hirshfeld tests on the cyanide groups for the beryllium and gallium compounds were indicated. After allowing the cyanide/isocyanide disordering to refine, the resulting CIF files gave acceptable Hirshfeld tests and marginally improved *R*-values for the beryllium ($R = 0.0397$ ordered, $R = 0.0326$ disordered) and gallium ($R = 0.0400$ ordered, $R = 0.0382$ disordered) compounds. Although unnecessary for the boron compounds, the disordered cyanide/isocyanide model was used for all the refinements for internal consistency.

Acknowledgment. This work was supported by the National Science Foundation. Computational studies were performed using the resources of the Fulton High Performance Computing Initiative at Arizona State University. It is a pleasure to acknowledge several discussions with Prof. George Wolf.

Supporting Information Available: CIF files for **1**–**4**. This material is available free of charge via the Internet at http://pubs.acs.org.

CM071275H